An adaptive temperature wall function for mixed convective flows at exterior surfaces of buildings in street canyons

Jonas Allegrini [a,*], Viktor Dorer [a], Thijs Defraeye[b], Jan Carmeliet [a,c]

[a] Laboratory for Building Science and Technology
Swiss Federal Laboratories for Materials Science and Technology (Empa)
Überlandstrasse 129, 8600 Dübendorf, Switzerland

[b] Division of Mechatronics, Biostatistics and Sensors, Department of Biosystems, Katholieke Universiteit Leuven, Willem de Croylaan 42, 3001 Heverlee, Belgium

[c] Chair of Building Physics, Swiss Federal Institute of Technology Zurich (ETHZ),
Wolfgang-Pauli-Strasse 15, 8093 Zürich, Switzerland

Abstract

For computational fluid dynamics (CFD) simulations of large urban areas the air flow near surfaces is normally modelled using Wall Functions (WFs). This study aims at improving the accuracy of WFs, in terms of heat transfer predictions. Turbulent boundary layers at heated building surfaces in a street canyon were analysed with low-Reynolds number modelling (LRNM). Buoyancy was accounted for, due to its importance in street canyons e.g. by solar radiation. Two extreme types of normalized temperature profiles could be identified in the thermal boundary layer dependent on the Richardson (Ri) number. One extreme at low Ri number could be attributed to forced convective flow, which is adequately described by existing standard wall functions (SWFs), and the second extreme at Ri>1 to mixed convective flows, where WFs adapted for non-equilibrium flows (NEWFs) are appropriate. Based on these two extremes, an adaptive temperature wall function (AWF) was derived that varies between the two existing WFs dependent on the local Ri. This AWF can account for the co-occurrence of forced and mixed convective flow regimes at a single surface. CFD simulations of street canyon configurations with SWF showed errors in the wall heat fluxes up to 60%, compared to the LRNM results, and up to 30% for NEWFs. With the proposed AWF, these errors were reduced to less than 10% for the majority of the cases studied over the whole range of Ri numbers. We conclude that the proposed AWF allows for more accurate convective heat transfer analysis in urban CFD studies.

Keywords

Convective heat transfer, Wall function, Computational fluid dynamics, Street canyon, Buoyancy, Mixed convection

[*] Corresponding author: Jonas Allegrini, Empa Dübendorf, Ueberlandstrasse 129, 8600 Dübendorf, Switzerland. Tel.: +41 (0) 58 765 47 21, Fax: +41 (0) 58 765 40 09, e-mail: jonas.allegrini@empa.ch

Nomenclature

c_p	specific heat capacity (J/kgK)
C_μ	turbulent-viscosity constant of the k-ε model
E	constant in wall function
g	gravitational acceleration (m/s^2)
h	reference height (m)
H	building height (m)
k	turbulent kinetic energy (m^2/s^2)
P_J	wall function constant
Pr	molecular Prandtl number
Pr_t	turbulent Prandtl number
Re	Reynolds number
Re^*	turbulent Reynolds number
Ri	Richardson number
Ri_{lo}	local Richardson number
T	temperature (K)
T_W	wall temperature (K)
T_P	temperature at the centre point P of the wall-adjacent cell (K)
T^*_P	dimensionless temperature at the centre point P of the wall-adjacent cell
T_0	reference temperature (K)
T^*	dimensionless temperature
u^*_{ABL}	ABL friction velocity (m/s)

u_P velocity at the centre point P of the wall-adjacent cell (m/s)

u^*_P dimensionless velocity at the centre point P of the wall-adjacent cell

U_{10} wind speed at 10 m above the ground (m/s)

U velocity (m/s)

u^* dimensionless velocity

$q_{c,w}$ convective heat flux at the surface (W/m^2)

x horizontal coordinate (m)

y vertical coordinate (m)

y_P wall distance of the centre point P of the wall-adjacent cell (m)

y^* dimensionless wall distance

y^*_P dimensionless wall distance at the centre point P of the wall-adjacent cell

y^+_P dimensionless wall distance at the centre point P of the wall-adjacent cell

z_0 aerodynamic roughness length (m)

Greek symbols

β volumetric thermal expansion coefficient (1/K)

κ von Karman constant

μ dynamic viscosity (kg/ms)

ν kinematic viscosity (m^2/s)

ρ density (kg/m^3)

ρ_0 reference density (kg/m^3)

ε turbulence dissipation rate (m^2/s^3)

τ_w wall shear stress (kg/ms^2)

Abbreviations

ABL	atmospheric boundary layer
AWF	adaptive wall function
CFD	computational fluid dynamics
CHTC	convective heat transfer coefficient
LES	large eddy simulation
LRNM	low-Reynolds number modelling
NEWF	non-equilibrium wall function
RANS	Reynolds-averaged Navier-Stokes
SWF	standard wall function
WF	wall function

Subscripts

$_P$	centre point of wall-adjacent cell

1. Introduction

Convective heat transfer can have a significant effect on the heat exchange at exterior building surfaces and thus also on the surface temperatures. The convective part of the total heat flux at the surface can be 2 to 7 times larger than the radiative component [1], and thus can be important for the thermal behaviour of a building. Convective heat transfer is especially important for glazed façade elements such as windows or double-skin façades [2], where the contribution of convective heat transfer to the overall thermal conductance of the building component is high due to its lower thermal resistance, and where heat fluxes at the surface also may be large due to high surface temperatures from solar irradiation. Accurate convective heat transfer predictions also become increasingly important for renewable energy system components mounted on or integrated into building roofs and façades, such as solar chimneys [3], solar collectors [4], and ventilated or building integrated photovoltaic panels [5, 6].

Local heat transfer predictions at building surfaces in general, including radiative fluxes, are not only of interest for the performance of the buildings but also for studying the effects on urban climate [7] and for thermal comfort assessment of urban outdoor spaces [8]. Modelling sensible heat fluxes from building surfaces is also important for urban canopy layer parameterizations in urban micro- and meso-scale models [9, 10]. Such models are employed to study urban heat island effects, which in return affect the building energy demand. Here, sunlit building façades with surface temperatures higher than the outside air temperature have a distinct influence on the local air flow patterns and the outdoor air temperature distribution due to buoyancy effects.

A large amount of measurements of the convective heat transfer at building façades were made by field tests, such as by Sharples [11], Hagishima and Tanimoto [12], Liu and Harris [13], and in wind tunnels, mostly on isolated cube models, e.g. by Nakamura et al. [14]. Overviews are given by Hagishima et al. [15], Defraeye et al. [16], and for building envelope energy systems by Palyvos [6]. Significant differences between the measured data can be found [16], because these data are very case specific and thus not general, which is however a prerequisite to use them as standard values.

More recently, convective heat transfer at building façades was investigated by numerical methods using computational fluid dynamics (CFD, e.g. [17, 18]). Compared to wind-tunnel experiments, numerical methods offer many advantages, such as larger flexibility in geometry and boundary conditions, a larger Reynolds (*Re*) number range, etc. However some limitations have to be emphasized. In order to limit the computational efforts for CFD simulations, (steady) Reynolds-averaged Navier-Stokes (RANS) methods are often applied, especially for complex building configurations, larger urban studies, combined indoor-outdoor air flow studies [19] or coupled building energy simulation (BES)-CFD simulations [20]. Even though e.g. large eddy simulations (LES) give more accurate results for flows in urban areas, RANS simulations are still used where LES are considered too calculation intensive. For example, correct average flow quantities can be obtained by LES only by considering very large numbers of time steps [21]. In addition, to simulate one year with a coupled BES-CFD simulation, preferably one CFD simulation for each BES time step (often 1 hour) has to be run. Therefore RANS simulations are often the preferred choice to get results within reasonable time. Here the boundary layer flow close to the surface is usually not resolved but modelled using wall functions (WFs) in order to reduce the computational cost. Alternatively, the boundary layer flow can be explicitly resolved by low-

Reynolds number modelling (LRNM), where the near-wall region is resolved down to the viscous sublayer. LRNM however requires an extremely high grid resolution at high Reynolds numbers. The standard formulation for WFs [22], referred to as standard wall functions (SWFs), however has two main limitations: (i) the cell centre point P of the wall-adjacent cell has to be located outside of the viscosity-affected region (viscous sublayer and buffer layer) (i.e. $y_P^+ > 30$), but on the other hand close enough to the wall in order to be within the logarithmic layer, (i.e. $y_P^+ < 500$) [23, 24]; (ii) SWFs are derived for wall-attached boundary layers under equilibrium conditions, i.e. small pressure gradients, local equilibrium between generation and dissipation of turbulent energy and a constant (uniform) shear stress and heat flux in the near-wall region. For flow with regions of separation, as is normally the case for flows around buildings, the SWF concept does not hold anymore. Although the overall flow field may not differ much from that calculated by more sophisticated approaches like LRNM, SWFs often lead to inaccurate predictions of wall friction and convective heat transfer [25]. Therefore a number of adjusted wall functions were proposed for non-equilibrium boundary layer flow, mainly in respect to velocity [26 - 28]. Defraeye et al. [29] proposed and validated such an adjusted temperature wall function for non-equilibrium forced-convective flows around buildings using LRNM. However, for the investigation of flow and heat transport in street canyons, at façades and building integrated solar components, accurate wall functions for mixed convection are needed, which consider buoyancy effects and their impact on the turbulence levels.

The aim of this paper is to determine improved thermal wall functions for flows including buoyancy at exterior building surfaces, to apply them to a 2D street canyon case and to compare these results with LRNM. The 2D street canyon is a rather academic geometry that was chosen to develop a methodology how WF can be adapted for buoyant flows in urban areas. It is possible to extend this methodology to other (more complex) geometries. First the temperature profiles in the near-wall region are studied for different Richardson numbers. It is found that the temperature profiles correspond well to the temperature profiles of standard wall functions if the flow is in a forced convective flow regime and to the temperature profiles of the adjusted wall function of Defraeye et al. [29] if it is in the mixed convective flow regime. Based on these results an adaptive temperature wall function (AWF) is derived that varies dynamically between the two types of temperature wall functions. The AWF is implemented in such a way that the temperature wall function regime is chosen separately (individually) for each wall adjacent cell of the computational grid. This AWF is used to model both forced and mixed convection in a 2D street canyon. In section 2 different approaches to model the near-wall region are discussed. Then a detailed description of the CFD simulations is given, followed by the results of the simulations with the different existing near-wall modelling approaches. Then, in section 7, the proposed AWF approach is described, and the respective simulation results using the AWF are given.

2. Near-wall modelling

2. 1. Low-Reynolds number modelling

Low-Reynolds number modelling (LRNM) is a method to model the flow in the boundary layer close to a wall surface. With LRNM, the near-wall region is resolved down to the viscous sublayer. Defraeye et al. [25] demonstrated that for the case of a cube immersed in a turbulent boundary layer the convective heat transfer predictions obtained with LRNM (steady RANS with realizable k-ε turbulence model) show a satisfactory agreement with the experimental data of Meinders et al. [30]. LRNM performs well in terms of convective

heat transfer determination, because the flow field (turbulent kinetic energy, velocity, temperature etc.) close to the walls is explicitly resolved. Based on detailed convective heat transfer measurements around the cube in a turbulent boundary layer reported by Meinders et al. [29], Defraeye et al. [24] performed a detailed validation of their CFD model. However, for buoyant flows in street canyons the data provided by the available experimental studies on convective heat transfer in street canyons are mostly not of sufficiently high spatial resolution for CFD validation purposes, or information relevant to CFD validation are lacking.

With the LRNM a two layer approach for the turbulent dissipation rate (ε) and the turbulent viscosity is used. In this study, in the fully-turbulent region the flow is resolved with the *k*-ε model, and in the viscosity-affected region the one-equation Wolfshtein model [31] is employed to compute ε and the turbulent viscosity. For distinction between the fully-turbulent and the viscosity-affected region the turbulent Reynolds number *Re** is used:

$$\mathrm{Re}^{*} = \frac{\sqrt{k}\,y}{\nu} \tag{1}$$

where *k* is the turbulent kinetic energy, *y* the normal distance from the wall and ν the kinematic viscosity. For *Re** < 200 the Wolfshtein model and for *Re** >200 the k-ε model is employed to calculate ε and the turbulent viscosity. The disadvantage of LRNM is that a very fine cell grid is required close to the wall to resolve the entire boundary layer, which leads to an increased computing time. Therefore, for CFD simulations of buildings in urban areas, wall functions are mostly used to cope with the complexity of the geometries and the size of computational domain. Another disadvantage is that no surface roughness can be used with LRNM. In this paper, we will assume that CFD simulations using LRNM are sufficiently accurate and can be used as reference solutions for evaluating results from different wall function approaches.

2.2. Standard wall function

Standard wall functions (SWFs) are used to save computing time by not resolving but modelling the flow in the viscous sublayer, the buffer layer and a part of the logarithmic layer. SWFs were derived for flows with a local equilibrium between the generation and dissipation of the turbulent kinetic energy, e.g. flat plate flow. The assumptions on which SWFs are based are usually not valid for complex flows, such as flows around bluff bodies, buoyancy driven flows or flows with large pressure gradients. Therefore SWFs can lead to inaccurate flow predictions for such non-equilibrium boundary layer flows.

For SWFs the centre point P of the wall-adjacent cell is placed inside the logarithmic layer and the flow parameters in the wall-adjacent cell centre are modelled by the law-of-the-wall. The profiles of dimensionless velocity *U** and the dimensionless temperature *T** as a function of the dimensionless wall distance *y** are universal in the near wall region for equilibrium boundary layer flows and can be described by the law-of-the-wall. These dimensionless parameters are related to the turbulent kinetic energy *k*:

$$y^{*} = \frac{\rho C_{\mu}^{1/4} k^{1/2} y}{\mu} \tag{2}$$

$$U^{*} = \frac{\rho C_{\mu}^{1/4} k^{1/2} U}{\tau_{w}} \tag{3}$$

$$T^* = \frac{\rho C_\mu^{1/4} k^{1/2} (T_w - T) c_p}{q_{c,w}} \quad (4)$$

where ρ is the air density, C_μ the turbulent viscosity constant, μ the dynamic viscosity, U a velocity, τ_w is the wall shear stress, T_w the wall temperature, T the considered temperature to be made dimensionless, c_p is the specific heat capacity and $q_{c,w}$ the convective heat flux at the wall.

The law-of-the-wall for the velocity, derived for equilibrium boundary layer flows and used by the SWFs, is linear in the viscous sublayer and logarithmic in the logarithmic layer:

$$U_P^* = y_P^* \qquad y_P^* < 11.225 \quad (5)$$

$$U_P^* = \frac{1}{\kappa} \ln(E y_P^*) \qquad y_P^* > 11.225 \quad (6)$$

where the subscript P refers to the point P, E is an empirical constant (9.793) and κ the von Karman constant (0.4187). The temperature law-of-the-wall for incompressible flows has a similar form:

$$T_P^* = \mathrm{Pr}\, y_P^* \qquad y_P^* < 11.639 \quad (7)$$

$$T_P^* = \mathrm{Pr}_t \left(\frac{1}{\kappa} \ln(E y_P^*) + P_J\right) \qquad y_P^* > 11.639 \quad (8)$$

where Pr and Pr_t are the molecular and turbulent Prandtl numbers and P_J is an empirically-determined coefficient, which is a function of Pr and Pr_t (here -1.12 for air). All the previously mentioned numerical values in Equations (5)-(8) are default values in ANSYS Fluent [24]. In ANSYS Fluent Pr_t is called the Wall Prandtl Number and can be specified for the wall independently from the turbulent Prandtl number used in the energy equation. The default Wall Prandtl Number in ANSYS Fluent is 0.85, and is used by the SWFs.

2.3. Non-equilibrium wall function

Defraeye et al. [25] studied the heat transfer at the surface of a cube immersed in a turbulent boundary layer. They found that the temperature law-of-the-wall of the SWFs is not valid for the bluff body cases they studied, due to non-equilibrium conditions of the flow (e.g. separation). They also found that although the law-of-the-wall for the velocity was not valid, the impact on the global flow field was however limited.

For their cases, Defraeye et al. [29] observed a universal behaviour of the dimensionless temperature in the boundary layer. In Figure 1 dimensionless temperature profiles of LRNM simulations are given for flows in street canyons, which correspond to the universal behaviour Defraeye et al. [29] observed. The results of their simulations with LRNM showed that for this type of non-equilibrium flow the temperature in the boundary layer also shows a logarithmic-like behaviour, consisting of two parts following line A and line B in Figure 1. Therefore they were able to derive a customized temperature wall function, here called non-equilibrium wall function (NEWF). This NEWF is based on fitting a logarithmic law, similar to Equation (8), to the LRNM data.

Defraeye et al. [29] proposed a way to implement the adjusted logarithmic law in ANSYS Fluent. Because it is only possible to adjust one parameter in Equation (8) in this code, namely Pr_t, an exact approximation of the

data (line A and B) could not be implemented. Therefore this NEWF can only be applied for y_P^* larger than 50. The best approximation with LRNM data was found for Pr_t = 1.95. With this NEWF for non-equilibrium boundary layer flows Defraeye et al. [29] improved the convective heat transfer at the walls significantly.

3. Importance of buoyancy

The NEWF by Defraeye et al. [29] was derived for bluff bodies in forced-convective turbulent boundary layers not considering buoyancy effects. In this study, the flow and heat transfer inside a street canyon is investigated. In figure 2, three characteristic flow types for two-dimensional street canyons can be distinguished. For forced convective flow (e.g. in a quasi isothermal case) one vortex is formed in a street canyon with flow normal to the street axis, as illustrated in Figure 2a. Buoyancy can however become important, e.g. during a sunny day with low wind speeds. The flow field in an urban street canyon can change completely due to buoyancy induced by high surface temperatures at the building façades, compared to the forced convective case. A second vortex (or even multiple vortices) can be formed due to buoyancy effects (e.g. [32] or [33]). Here, we denote this case as mixed convection (Figure 2c). There exists also intermediate states, where the flow pattern mainly resembles that of the forced convective case but where the influence of buoyancy on the local flow field can already be noticed (Figure 2b), here denoted as the intermediate convective case. Buoyancy thus has a strong impact on the specific microclimate that develops in a street canyon and on the convective heat transport at the building façades. Due to buoyancy also the turbulence in the street canyon is increased, which enhances the convective heat transport at the walls, as will be shown below.

4. Numerical model

In this study we first analyse a 2D street canyon in an atmospheric boundary layer (ABL), extending later to the three dimensional case. The size of the computational domain (Figure 3) is determined according to the guidelines of Franke et al. [23]. The street canyon is modelled as a cavity of 10m width (W) and 10m (H) height, thus with an aspect ratio (H/W) of 1.

At the inlet of the domain vertical profiles of the mean horizontal wind speed U (logarithmic law), turbulent kinetic energy (k) and rate of dissipation of turbulent kinetic energy (ε) are imposed according to Richards and Hoxey [34]. These profiles represent a neutral ABL, where the turbulence originates only from friction and shear:

$$U(y) = \frac{u^*_{ABL}}{\kappa}\ln\left(\frac{y+z_0}{z_0}\right)$$
$$k = \frac{u^{*2}_{ABL}}{\sqrt{C_\mu}} \qquad (9)$$
$$\varepsilon = \frac{u^{*3}_{ABL}}{\kappa(y+z_0)}$$

where u^*_{ABL} is the ABL friction velocity, y the height above the ground, z_0 is the aerodynamic roughness length (here 0.03m). By imposing this type of approach flow, the street canyon is modelled as a cavity within an ABL with low approach flow roughness, instead of as a cyclic reoccurring street canyon. The approach flow

conditions for the latter are often obtained by employing cyclic boundary conditions. The choice for the type of approach flow was made with the perspective on future wind-tunnel tests on buoyancy effects. For these tests, a large scale model will be constructed to obtain Richardson similarity, by which approach flow conditions for cyclic reoccurring street canyon configurations cannot be obtained in the wind tunnel. The methodology developed in this paper could however easily be extended to more complex geometries like a row of street canyons. Note that the applied roughness is chosen rather low to limit the gradient in the vertical profiles of the mean horizontal wind speed, as for LRNM simulation in general no roughness can be specified. For this study the ABL friction velocity is determined with the logarithmic law (Equation (9)) for different reference wind speeds U_{10} between 0.5m/s and 5m/s. U_{10} is the mean approach-flow wind speed at 10m above the ground (y = 10m). At the inlet a constant temperature of 10°C is imposed.

At the ground surface a no-slip boundary condition with zero roughness is used, because no surface roughness can be specified for LRNM in ANSYS Fluent [23]. In order to correctly compare the simulations using WF with the simulations using LRNM, also for the simulations with WF no roughness is specified. Therefore a gradient in the vertical profiles of the mean horizontal wind speed, k and ε cannot be avoided, but is rather limited because a short upstream fetch is considered [34]. By conducting CFD simulations with WFs and roughness it was found that this change in the ABL causes only small differences of the flow inside the street canyon and therefore also of the wall heat fluxes at the building façades. The ground in front and behind the street canyon is modelled adiabatic. At the ground of the street canyon different constant temperatures between 10.5-50°C are imposed. For the building walls in the street canyon a no-slip boundary condition with zero roughness is used. Different constant temperatures between 10.5-50°C are imposed at the walls. Surface temperatures of ground and walls are always identical. So, it is important to remark that we consider the surface temperatures in the street canyon to be constant over space and time.

At the top boundary, a symmetry boundary condition is applied, assuming that there are no normal velocities or normal gradients at this boundary. At the outlet an outflow boundary condition is used, which assumes that there are quasi no streamwise gradients at the outlet.

A 2D structured grid is build based on a grid sensitivity analysis and the guidelines of Franke et al. [23]. The grid consists of 17300 cells for the simulations with LRNM and of 4900 cells for the simulations with wall function modelling. The grids are refined towards the wall to resolve the boundary layers. For the LRNM simulations the highest y_p^+ values, i.e. at the highest wind speed, are <4 and for the simulations with WFs, they are <300. According to user's guide of Fluent 2009 [24] the y_P^+ has to be <5 for the LRNM and <300 (and >30) for WFs.

5. Numerical simulation

For this study CFD simulations are conducted using ANSYS Fluent 12.0 [24] which uses the control volume method. 2D steady incompressible RANS simulations with the realizable k-ε model [36] are performed. The near wall regions are either resolved with LRNM as described in section 2.1., or modelled with different WFs. Pressure-velocity coupling is taken care of by the SIMPLEC algorithm. The PRESTO spatial discretization scheme is used for the pressure interpolation and second order spatial discretization schemes are used for

the convection of the governing equations. Radiation is not considered in the CFD simulations, since constant temperature boundary conditions are applied on the street canyon surfaces.

To account for buoyancy the Boussinesq approximation is used. With the Boussinesq approximation a constant value for the density is used for all equations except for the buoyancy term in the momentum equation:

$$\rho = \rho_0(1 - \beta(T - T_0)) \tag{10}$$

where ρ_0 is a reference density, β is the volumetric thermal expansion coefficient, T is the temperature of the flow and T_0 is the reference temperature. The Boussinesq approximation is only valid for small density changes in the flow field ($\beta(T - T_0) << 1$). For the simulations of this study the maximum value for $\beta(T - T_0)$ is 0.14.

As mentioned, simulations with different WFs are compared with LRNM, which we consider as reference results. Xie et al. [37] validated their CFD model for a street canyon with the experimental data from Uehara et al. [38]. In this study, the CFD model of the street canyon is similar to the one of Xie et al. They used ANSYS Fluent to run 2D RANS simulation with the realizable k-ε turbulence model and used the Boussinesq approximation to account for buoyancy. LRNM was used to resolve the near wall region. They found that the temperature and horizontal velocity profiles along the vertical centreline of the CFD simulations were comparable with the wind tunnel measurements of Uehara et al. [38]. Above the roof level the horizontal velocities of the CFD simulations were lower than the velocities from the measurements. They claim that the reason for this were the inflow profiles, which were slightly different from the profiles of the experiment. Based on the validation studies of Xie et al. [37] and Defraeye et al. [25] it can be assumed that the LRNM simulations can accurately predict the heat transfer for the case considered in this study, and as such we can consider our LRNM results sufficiently accurate to be used as reference solutions.

In this study the buoyancy forces are caused by air density changes due to the heated building façades. To decide whether buoyancy forces have to be accounted for, a 'global' Richardson number (*Ri*) is used:

$$Ri = \frac{g\beta(T_W - T_0)h}{U^2} \tag{11}$$

where g is the gravitational acceleration, T_w the wall temperature, h a reference height (here the building height H), U a reference velocity (here the reference velocity U_{10}) and T_0 a reference temperature (here the temperature at the inlet boundary) . For very low Richardson numbers (forced convection) the buoyancy forces can be neglected. For *Ri* around 1 (mixed convection) the mechanical and the buoyancy forces are both important. For very high Richardson numbers (natural convection) the mechanical forces can be neglected. In this study CFD simulations with Richardson number from 0.14 to 13.7 were conducted, for different combinations of wind velocity and temperature difference (Table 1).

6. Results with different near-wall modelling approaches

6.1. Dimensionless temperature profiles in the near-wall region

In this section, results of the LRNM simulations for global Richardson numbers from 0.14 to 13.7 (Table 1) are presented. In Figure 4, the profiles for the dimensionless temperature (a,b) and turbulent kinetic energies (c,d) along the horizontal centreline (Figure 3b) for two simulations with different global Richardson numbers (0.34 and 3.4) are given for the leeward (a,c) and the windward wall (b,d) in a street canyon. Mainly two types of dimensionless temperature profiles were found close to the wall. For the simulation with global Ri = 0.34 the dimensionless temperature profiles follow the law-of-the-wall of the SWFs for both leeward and windward wall. The dimensionless temperature profiles of the simulation with global Ri = 3.4 follow the non-equilibrium approximation derived by Defraeye et al. [29]. We remark that for some flow fields y^* decreases after some distance from the wall, which can be explained by the fact that the square root of k in Equation 2 is decreasing faster than y is increasing.

Further it can be observed that the shapes of the turbulent kinetic energy profiles in the boundary layer are different for the two global Ri numbers. For the flow with low global Ri the turbulent kinetic energy is increasing in the viscous sublayer ($y^* < 100$) due to the velocity gradient. Further away from the wall the turbulent kinetic energy is decreasing again. This behaviour is similar to the behaviour of a flat plate flow (Figure 5), for which the SWFs were originally derived. In Figure 4c and 4d the turbulent kinetic energy is moderately increasing at higher distance from the wall due to the higher turbulent kinetic energies in the centre of the street canyon. Because the flow inside the street canyon with low global Ri is similar to a flat plate flow and the law-of-the-wall was derived for a flat plate flow, the dimensionless temperatures are approximately similar to the law-of-the-wall. Therefore also the wall heat fluxes calculated with the SWFs correspond to the wall heat fluxes simulated with LRNM, as will be shown further below.

For the simulation with the higher global Ri, the turbulent kinetic energy is monotonically increasing in the boundary layer. This monotonic increase of turbulent kinetic energy is caused by the high turbulence level further away from the walls inside the street canyon due to buoyancy. In an urban street canyon with mixed convection (global Ri>1) an important part of the turbulent kinetic energy is produced by buoyancy and therefore the law-of-the-wall derived for equilibrium boundary layer flows is not applicable anymore. For this type of non-equilibrium boundary layer flows a quasi universality of the dimensionless temperature profiles can be found, as shown below, which can be used to determine a NEWF as described in section 2. Such dimensionless temperature profiles were described by Defraeye et al. [29], who determined a NEWF that improves the results for non-equilibrium boundary layer flows especially in terms of the wall heat fluxes.

Figure 6 shows the dimensionless temperature profiles along the horizontal centreline of different simulations with global Ri numbers from 0.14 to 13.7. For almost all the simulations with global Ri<1 the dimensionless temperature profiles follow the law-of-the-wall and for almost all the simulations with global Ri>1 the dimensionless temperature profiles follow non-equilibrium approximation.

It can be concluded that, for a flow in a street canyon with constant surface temperatures in space and time, two extreme types of dimensionless temperature profiles exist for the whole range of global Richardson numbers. The two extreme cases can be described by the either SWFs or NEWFs. The global Ri number can be used be to distinguish between these two types.

6.2. Forced convection case

For forced convection or equilibrium flows the SWFs performs better, because of the reasons explained above. In Figure 7 the convective heat transfer coefficients (CHTCs), defined as wall heat flux divided by the temperature difference between the surface and the uniform inlet temperature, for simulations with global Ri = 0.14 are given for LRNM, SWFs and NEWF. In this case the results with the SWFs agree better with the LRNM results than the results with the NEWF, as expected. The NEWF underestimates the CHTCs.

6.3. Mixed convection case

In Figure 8, the CHTCs at the leeward and windward wall for SWFs and NEWF are compared with LRNM for a global Ri = 3.4. It can clearly be noticed that the results with the NEWF show a much better agreement with the LRNM results than the results with the SWFs.

This is what was expected by the analysis of the dimensionless temperature profiles for the same boundary conditions in the section 6.1. In Figure 9 profiles of the dimensionless temperature for different heights above the ground of the street canyon are given. These profiles do correspond to the non-equilibrium approximation for all heights, and not only for the centreline given in Figure 6. There is however an underestimation of the wall heat flux close to the ground (y/H < -0.8). This underestimation is caused by the interaction with the ground surface and cannot be avoided because the flow fields with the WFs and the LRNM are different here.

Figure 10 shows the turbulent kinetic energy profiles along the horizontal (a) and the vertical centreline (b) for the three near wall modelling approaches. It can be noticed that for the SWFs the turbulent kinetic energies are too high in the street canyon. The turbulent kinetic energy profiles with the NEWF agree better with the LRNM results than the ones with the SWFs. Therefore with the NEWF not only the temperature field and the calculation of the wall heat fluxes can be improved, but also the flow field characteristics. For the study of Defraeye et al. [29] the use of the NEWF did not have any influence on the flow field, because buoyancy was neglected. In this study buoyancy is accounted for and therefore the thermal field predictions also influence the turbulent kinetic energies and the velocities inside the street canyon.

6.4. Intermediate convection case

For intermediate convection cases (Figure 2) the dimensionless temperature profiles corresponds in a part of the street canyon to the law-of-the-wall and in other parts to non-equilibrium approximation. As an example results for a simulation with a global Ri = 0.38 are shown in Figure 11. Here the profiles of the dimensionless temperature are given for different heights above the ground of the street canyon for the leeward (a) and the windward wall (b). Close to the ground the profiles correspond to the non-equilibrium approximation. Above y/H = -0.8 the profiles correspond to the law-of-the-wall. For this convection case it is not possible to choose one single temperature WF for the whole domain. The temperature WF has to be chosen locally, namely dependent on the local flow field characteristics. To solve this problem an adaptive WF is proposed in this paper.

7. Adaptive wall function

7.1. Concept of the adaptive wall function

As stated in the previous section, two types of temperature profiles corresponding to equilibrium and non-equilibrium boundary flows can be found in street canyons depending on the Richardson number. Therefore different wall function types should be used at different Richardson numbers to correctly simulate the heat exchange between the surface and the fluid. A criterion is thus needed for the selection of the appropriate WF type, based on the local flow field. A local Richardson number Ri_{lo} is therefore proposed:

$$Ri_{lo} = \frac{g\beta(T_W - T_P)h}{u_P^2} \tag{12}$$

where T_P is the temperature in the wall-adjacent cell centre and u_P the velocity magnitude here. This Ri_{lo} number has the advantage that it evaluates the importance of buoyancy very locally and close to the wall, i.e. where the heat exchange of the surface with the flow occurs. In contrast, the global Richardson number usually is defined by a free stream velocity and temperature and thus evaluates the importance of buoyancy on the street canyon or building scale. This reference temperature and velocity are not necessarily representative for the flow close to the surface, where the heat exchange takes place. Furthermore, we found that the local Richardson number is quasi grid-insensitive in the y* range, where the wall functions can be applied.

In this section we investigate for which local Richardson number the temperature profiles correspond to those of equilibrium and to non-equilibrium boundary layer flows respectively. From these simulations an empirical relationship for the turbulent Prandtl number Pr_t as a function of the local Richardson number is derived (Figure 12). The adaptive wall function (AWF) is built up in following way. For local Richardson numbers below 1 the SWFs are used and therefore the wall Prandtl number is equal to the default value of 0.85 (in ANSYS Fluent). For local Richardson numbers between 1 and 6 a transition from forced to mixed convection is modelled by linear interpolation. For local Richardson numbers larger than 6 the NEWF with Pr_t = 1.95 is used. To determine the Ri_{lo} limits (Ri_{lo} < 1 and Ri_{lo} > 6) of the mixed and forced convection cases, simulations with different Ri_{lo} limits were run. As a lower limit Ri_{lo} between 0.5 and 4 and as an upper limit Ri_{lo} between 4 and 10 were used. Based on the least-squares method the optimum was found to be 1 for the lower limit and 6 for the upper limit.

The local Richardson number is found to be quasi grid-insensitive in the y* range, where the wall functions can be applied: Ri_{lo} is almost constant in this range, except for some special cases, where the local Richardson numbers are much higher than 6 and therefore the NEWF has to be used anyway.

In the CFD code used in this study (ANSYS Fluent 12.0), the local Richardson number concept was implemented by means of a user-defined function. For each wall-adjacent cell the local Richardson number is computed during each iteration and the wall Prandtl number is set according to the local Richardson number. Note that even if the wall Prandtl number changes for some cells between two iterations the simulations were found not to become unstable.

7.2. Results of the adaptive wall function

In Figure 13 the CHTCs from simulations with global Ri = 0.38 are given for different near-wall treatments for the leeward and the windward wall. It can be noticed that for the leeward wall the NEWF underestimates and the SWF overestimates the CHTCs. The results with the AWF with the local Richardson number concept show a much better agreement with the LRNM results.

For the windward wall the AWF is in better agreement with the LRNM results, except for the region close to the ground. This is due to fact that in this region the WFs and the LRNM predict different flow fields.

For the different combinations of wind speeds and temperatures and thus different global Richardson numbers (see Table 1), simulations were conducted with the three WF types presented here. The results of these simulations were compared with results of the LRNM simulations. Figure 14 gives the deviations from the LRNM results (total wall heat flux) for the three wall function types (normalised by the LRNM results). The total wall heat flux is a conservative choice to compare the results of the simulations with different wall modelling approaches. The deviations would be even larger if the sum of the absolute value of the deviations at each location would be compared.

The SWFs overestimate the wall heat flux for all the studied cases for both walls. For cases with a global Ri > 1 the overestimation is between 10-20%. This overestimation is mainly due to regions at the walls, where dimensionless temperature profiles correspond to the non-equilibrium approximation. This can clearly be seen in Figure 7. For cases with a global Ri < 1 the SWFs overestimates the wall heat flux by 30-60% for both walls. For cases with a global Ri < 1, the NEWFs underestimate the wall heat flux up to 20%. The new proposed AWF performs better than the SWFs and the NEWF for all the studied cases. The deviation from the LRNM is less than 10% for almost all cases. This is a significant improvement compared to the deviation of the NEWF (up to 30%) and the deviation of the SWFs (up to 60%). For global Ri = 0.68 the accuracy of the AWF is significantly less than for all the other global Ri numbers. The reason for this higher deviation is that this case is in the transition zone between the SWFs and the NEWF (local Ri_{lo} at almost all parts of the wall are between 1 and 6) for almost the whole domain, which uses a simplified linear interpolation. In this transition zone the convective heat transfer is very sensitive to small changes in the flow field.

7.3. 3D street canyon

The proposed AWF was also used for a 3D street canyon simulation to investigate whether the AWF also performs well for 3D geometries with oblique winds. Therefore the 2D street canyon was elongated to a 50m long street canyon and periodic boundary conditions were used at the lateral boundaries. For the simulations, wind at a 45° angle to the street axis was considered. In Figure 15 the profiles of the CHTCs are given at the centre (normal to the x-y plane of Figure 3b) of the elongated street canyon. For this particular case (global Ri = 3.4) the AWF gives better results than the other two WFs. Further investigations have to be conducted for other 3D geometries to confirm that the AWF can be generally used for 3D street canyons.

8. Discussion

A new wall function, called adaptive WF (AWF) was derived which varies adaptively at each location on the wall surface between two existing WF types, based on the local Richardson number. This methodology was developed for a 2D street canyon, but it is possible to extend it to other (more complex) geometries. The AWF is easy to implement in existing CFD codes (for example in ANSYS Fluent). For the studied cases, the AWF results deviate less from the LRNM results than the results of the other two WF types and the AWF is applicable for both forced and mixed convection. However this new wall function has some limitations, which are given here:

- This study was conducted for a two-dimensional geometry. The derived AWF is expected to be valid also for three-dimensional geometries, because the same phenomena will occur here regarding the impact of buoyancy on the profiles of the dimensionless temperature and dimensionless velocity, normal to the surfaces. The AWF was tested for one 3D street canyon with an oblique flow direction. First results indicate that the AWF is also valid for these flow fields. This conclusion has however to be confirmed by simulating a larger number of urban configurations.
- This study is performed for one specific geometric configuration, namely a symmetric street canyon, where the flow field of the WFs agrees well with the flow field of LRNM. For cases where WFs fail to predict the correct flow field on a building scale, e.g. for cylindrical buildings, it will not be possible to get the correct heat fluxes with these WFs.
- Since the NEWF is only applicable for y_P^* above about 50, this limitation holds also for the AWF, as the NEWF formulation is an integral part of the AWF.
- The AWF is based on simulations using the realizable k-ε model and therefore the values of the used parameters (Pr and local Richardson number) should be used in combination with this turbulence model. The proposed AWF is however also expected to perform well with other similar turbulence models, such as the standard k-ε model. The used parameters might have to be adjusted for other turbulence models.
- The AWF presented was derived focusing on buoyant flows in street canyons. Therefore the local Richardson number is used as a criterion to choose between the SWF and the NEWF. However, the local Richardson number does not account for the turbulent kinetic energy which is important for the heat transfer. In future work, cases will be modelled with increased turbulence level inside the street canyon and on the building façade not only due to buoyancy but also due to advection (3D cases) or due to more detailed façade details (balconies, window sills etc.). This will have an influence on the heat transfer and thus on the selection of the WF and thus may have to be considered in future developments of AWFs.

9. Conclusion

Thermal boundary layers on building walls in street canyons were studied by CFD simulations accounting for buoyancy with the aim to improve the existing wall functions (WFs) for convective heat transfer predictions. Low-Reynolds number modelling (LRNM) of the transport in the boundary layer was used as a reference solution to evaluate the performance of different WF types. First the dimensionless temperature profiles and the turbulent kinetic energy profiles were analysed. Two main types of dimensionless temperature profiles could be identified. One of these dimensionless temperature profiles corresponds to the temperature law-of-the-wall as used in standard wall functions (SWFs). The second dimensionless temperature profile corresponds to a customized thermal WF for flows with non-equilibrium boundary layers (called NEWF). Both boundary layer types can be observed in a street canyon with buoyant flow. For forced convective flows at the surfaces the SWFs provide most accurate heat transfer predictions and for mixed convective flows the simulations using NEWFs are most accurate. Based on this observation, an adaptive wall function (AWF) was

derived that interpolates between the two existing WF types dependent on the local Richardson number, proposed in this paper. For the determination of the local Richardson number, the temperature and the velocity magnitude in the cell adjacent to the wall are used as reference temperature and velocity. The AWF can be used for mixed and forced convection whereas the SWFs only provides relatively accurate heat transfer results for forced convective street canyon flow and the NEWF for mixed convective street canyon flow. For the AWF, the deviations from the total heat flux of LRNM are less than 10% for almost all cases analysed. For the SWFs these deviations are between 10% and 60% and for the NEWF up to 30%. Apart from the limitations discussed above, the AWF approach has shown to be a valuable technique for the simulation of flow fields and convective heat transport in urban street canyons in cases where buoyancy plays an important role. This AWF approach shows the potential to importantly increase the accuracy of convective heat transfer predictions in CFD studies in the urban context. Even though LRNM performs better for simulations with convective heat transport, accurate WF are often the only option for large-scale urban engineering studies, where complex geometries, grid generation and computing power limitations become a limiting issue.

Acknowledgments

Funding by the Swiss Federal Office of Energy (SFOE) is gratefully acknowledged.

References

[1] Davies MG. Building heat transfer. 1st ed. Chichester: John Wiley & Sons Ltd.; 2004.

[2] Chou SK, Chua KJ, Ho JC. A study on the effects of double skin façades on the energy management in buildings. Energ Convers Manage 2009;50(9):2275-81.

[3] Harris DJ, Helwig N. Solar chimney and building ventilation. Appl Energy 2007;84:135-46.

[4] Sharples S, Charlesworth PS. Full-scale measurements of wind-induced convective heat transfer from a roof-mounted flat plate solar collector. Sol. Energy 1998;62 (2):69-77.

[5] Tian W, Wang Y, Xie Y, Wu D, Zhu L, Ren J. Effect of building integrated photovoltaics on microclimate of urban canopy layer. Build Environ 2007;42 (5):1891-1901.

[6] Palyvos JA. A survey of wind convection coefficient correlations for building envelope energy systems' modeling. Appl Therm Eng 2008;28(8-9):801-8.

[7] Ooka R. Recent development of assessment tools for urban climate and heat-island investigation especially based on experiences in Japan. Int. J. Climatol 2007;27:1919–30.

[8] Mayer H, Holst J, Dostal P, Imbery F, Schindler D. Human thermal comfort in summer within an urban street canyon in Central Europe. Meteorologische Zeitschrift 2008;17(3):241-50.

[9] Tokairin T, Kondo H, Yoshikado H, Genchi Y, Kikegawa Y, Hirano Y, Asahi K. Numerical Study on the Effect of Buildings on Temperature Variation in Urban and Suburban Areas in Tokyo. JMSJ 2006;84(5):921-37.

[10] Salamanca F, Krpo A, Martilli A, Clappier A. A new building energy model coupled with an urban canopy parameterization for urban climate simulations-part I. formulation, verification, and sensitivity analysis of the model. Theor Appl Climatol 2010;99(3-4):331-44.

[11] Sharples S. Full-scale measurements of convective energy losses from exterior building surfaces. Build Environ 1984;19(1):31-9.

[12] Hagishima A, Tanimoto J. Field measurements for estimating the convective heat transfer coefficient at building surfaces. Build Environ 2003;38(7):873-81.

[13] Liu Y, Harris DJ. Full-scale measurements of convective coefficient on external surface of a low-rise building in sheltered conditions. Build Environ 2007;42(7):2718-36.

[14] Nakamura H, Igarashi T, Tsutsui T. Local heat transfer around a wall-mounted cube in the turbulent-boundary layer. Int J Heat Mass Tran 2001;44(18):3385-95.

[15] Hagishima A, Tanimoto J, Narita KI. Intercomparisons of experimental convective heat transfer coefficients and mass transfer coefficients of urban surfaces. Boundary-Layer Meteorol 2005;117(3):551-76.

[16] Defraeye T, Blocken B, Carmeliet J. Convective heat transfer coefficients for exterior building surfaces: Existing correlations and CFD modelling. . Energ Convers Manage 2011;52:512–22.

[17] Blocken B, Defraeye T, Derome D, Carmeliet J. High-resolution CFD simulations for forced convective heat transfer coefficients at the façade of a low-rise building. Build Environ 2009;44(12):2396-412.

[18] Defraeye T, Carmeliet J. A methodology to assess the influence of local wind conditions and building orientation on the convective heat transfer at building surfaces. Environ Modell Softw 2010;25(12):1813-24.

[19] van Hooff T, Blocken B. Coupled urban wind flow and indoor natural ventilation modelling on a high resolution grid: a case study for the Amsterdam ArenA stadium. Environ Modell Softw 2010;25(1):51-65.

[20] Chen H, Ooka R, Huang H, Tsuchiya T. Study on mitigation measures for outdoor thermal environment on present urban blocks in Tokyo using coupled simulation. Build Environ 2009;44:2290–9.

[21] Moonen P, Gromke C, Dorer V, Carmeliet J. LES of dispersion in a street canyon with tree planting. International Workshop on Physical Modelling of Flow and Dispersion Phenomena, Hamburg, Germany; 2011.

[22] Launder BE, Spalding DB. The numerical computation of turbulent flows. Comput Method Appl M Eng 1974;3(2):269-89.

[23] Franke J, Hellsten A, Schlünzen H, Carissimo B. Best practice guideline for the CFD simulation of flows in the urban environment, COST Action 732: Quality assurance and improvement of microscale meteorological models. Hamburg, Germany; 2007.

[24] Fluent. Fluent 12.0 User's Guide; 2009. Lebanon - New Hampshire. USA.

[25] Defraeye T, Blocken B, Carmeliet J. CFD analysis of convective heat transfer at the surfaces of a cube immersed in a turbulent boundary layer. Int J Heat Mass Tran 2010;53(1-3):297-308.

[26] Balaji C, Hölling M, Herwig H. A temperature wall function for turbulent mixed convection from vertical, parallel plate channels. Int J Therm Sci 2008;47(6):723-9.

[27] Craft TJ, Gant SE, Iacovides H, Launder BE. A new wall function strategy for complex turbulent flows. Numer Heat Tr B - Fund 2004;45(4):301-318.

[28] Popovac M, Hanjalic K. Compound wall treatment for RANS computation of complex turbulent flows and heat transfer. Flow Turbul Combust 2007;78(2):177-202.

[29] Defraeye T, Blocken B, Carmeliet J. An adjusted temperature wall function for turbulent forced convective heat transfer for bluff bodies in the atmospheric boundary layer. Build Environ 2011; doi:10.1016/j.buildenv.2011.04.013.

[30] Meinders ER, Hanjalic K, Martinuzzi RJ. Experimental study of the local convection heat transfer from a wall-mounted cube in turbulent channel flow. T ASME: J Heat Trans 1999;121(3):564-573.

[31] Wolfshtein M. The velocity and temperature distribution in one-dimensional flow with turbulence augmentation and pressure gradient. Int J Heat Mass Tran 1969;12(3):301-18.

[32] Kovar-Panskus A, Moulinneuf L, Savory E, Abdelqari A, Sini JF, Rosant JM, Robins A, Toy N. A wind tunnel investigation of the influence of solar-induced wall-heating on the flow regime within a simulated urban street canyon. Water Air Soil Pollut 2002; Focus 2:555-71.

[33] Xie, X, Liu CH, Leung YC. Impact of building façades and ground heating on wind flow and pollutant transport in street canyons. Atmos Environ 2007;41:9030-49.

[34] Richards PJ, Hoxey RP. Appropriate boundary conditions for computational wind engineering models using the k-3 turbulence model. J Wind Eng Ind Aerod 1993;46-47:145-53.

[35] Blocken B, Stathopoulos T, Carmeliet J. CFD simulation of the atmospheric boundary layer: wall function problems. Atmos Environ 2007;41(2):238-52.

[36] Shih TH, Liou WW, Shabbir A, Yang Z, Zhu J. A new k-ε eddy viscosity model for high Reynolds number turbulent flows. Comput Fluids 1995;24(3):227-238.

[37] Xie X, Liu CH, Leung YC, Leung KH. Characteristics of air exchange in a street canyon with ground heating. Atmos Environ 2006;40:6396-409.

[38] Uehara K, Murakami S, Oikawa S, Wakamatsu S. Wind tunnel experiments on how thermal stratification affects flow in and above urban street canyons. Atmos Environ 2000;34:1553–62.

[39] Spalart PR. Direct simulation of a turbulent boundary layer up to R_θ=1410. J Fluid Mech 1988;187:61-98.

Figure Captions

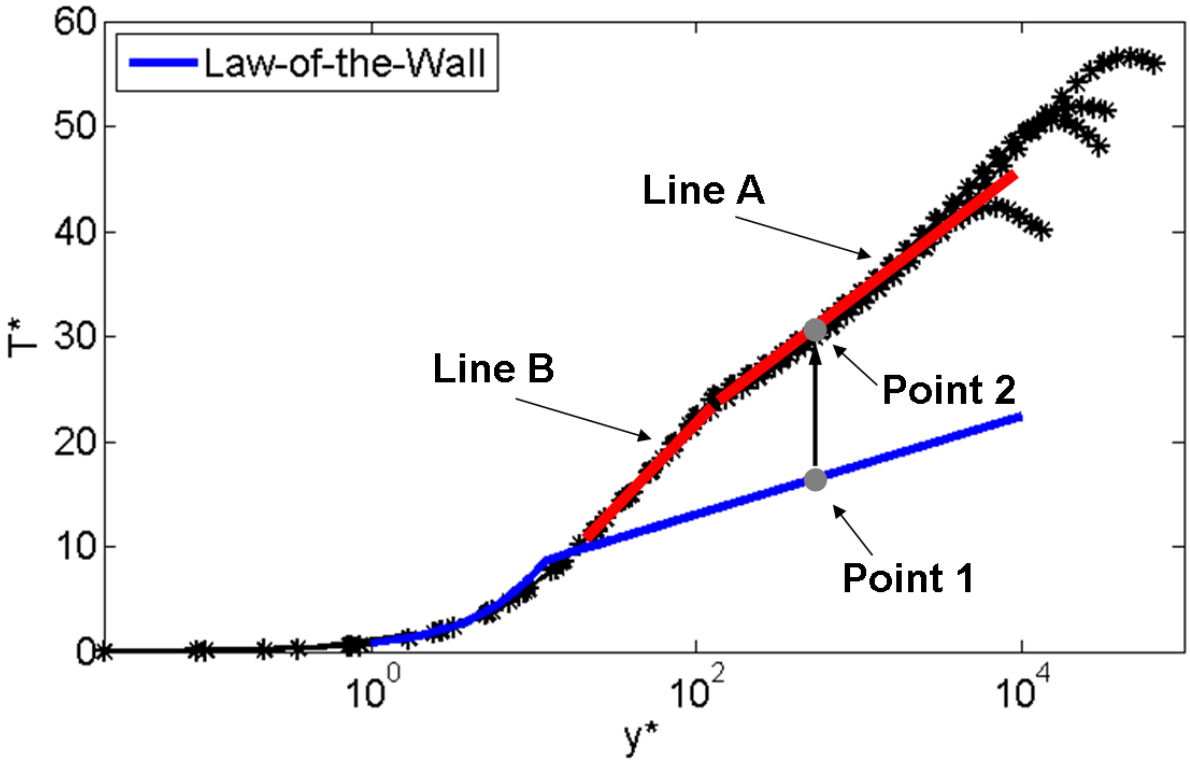

Figure 1: Dimensionless temperature profiles of LRNM simulations of non-equilibrium flows in street canyons as a function of the y* value; Blue: temperature law-of-the-wall; Red: logarithmic approximations.

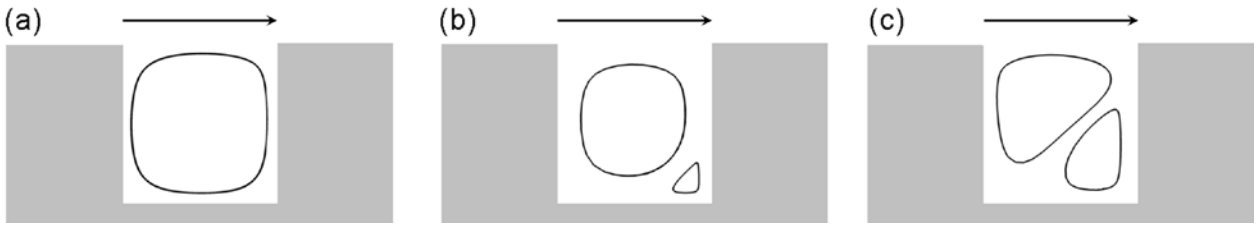

Figure 2: Streamlines of forced convective (a), intermediate convective (b) and mixed convective (c) cases.

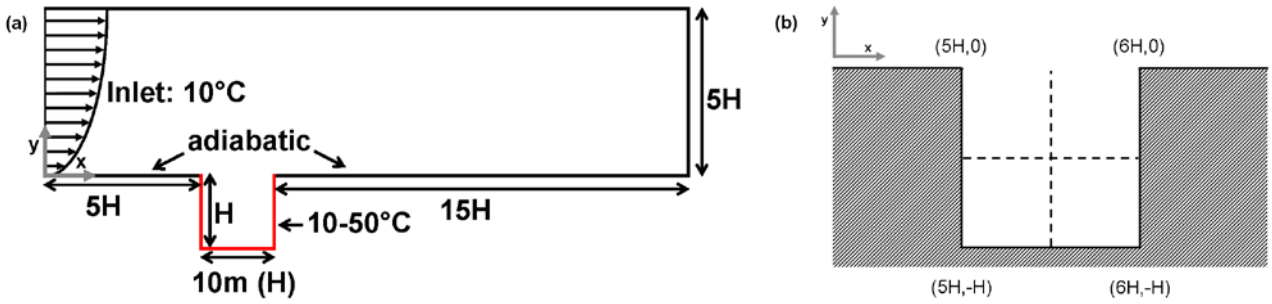

Figure 3: Computational domain (a); Horizontal and vertical centrelines in the street canyon (b). In all figures *y** ranges from the surface to the intersection of the horizontal and the vertical centrelines.

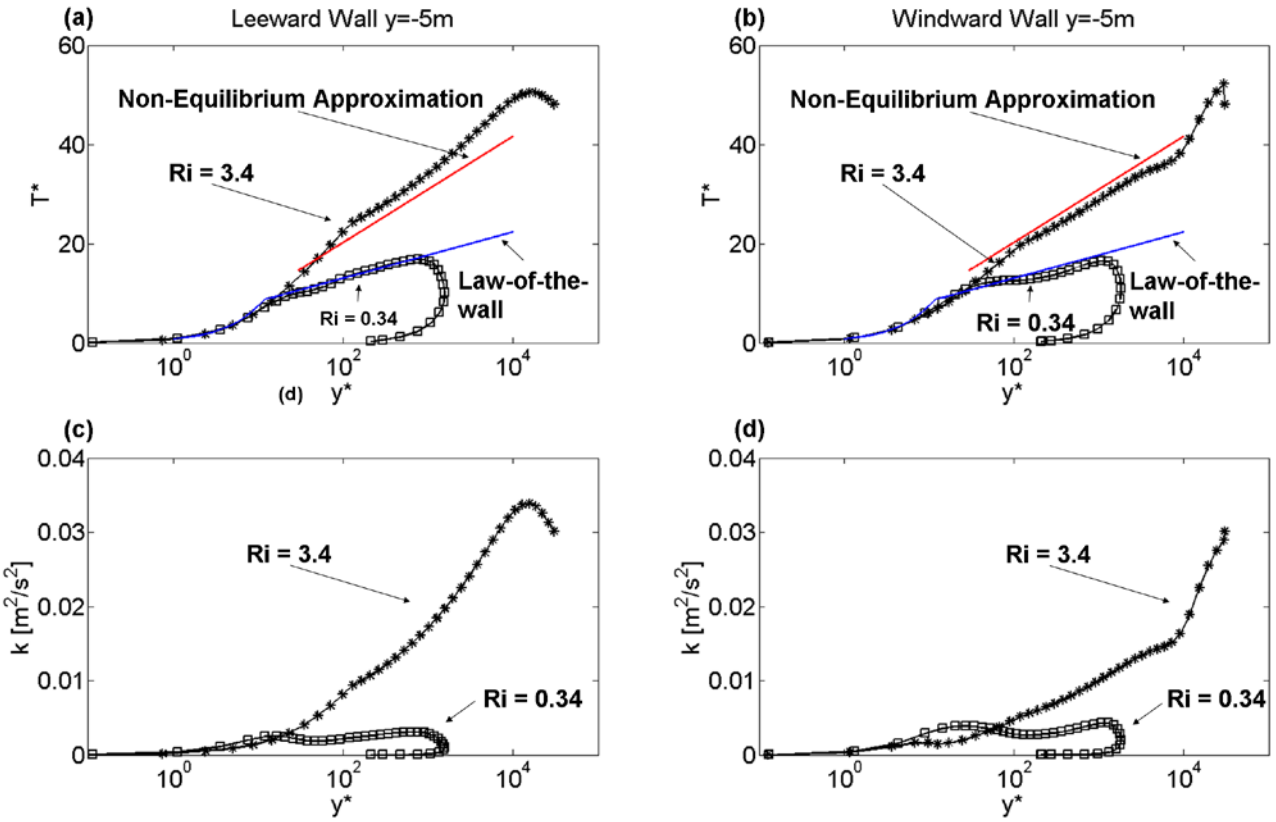

Figure 4: Dimensionless temperature profiles and turbulent kinetic energy profiles as a function of the *y** value on the horizontal centreline (see Figure 3b) of a street canyon for two simulations with different global *Ri* numbers (0.34 and 3.4).

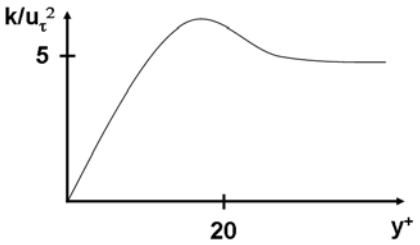

Figure 5: Schematic representation of the turbulent kinetic energy, scaled with the friction velocity as a function of the y^+ value for flat plate flow [39].

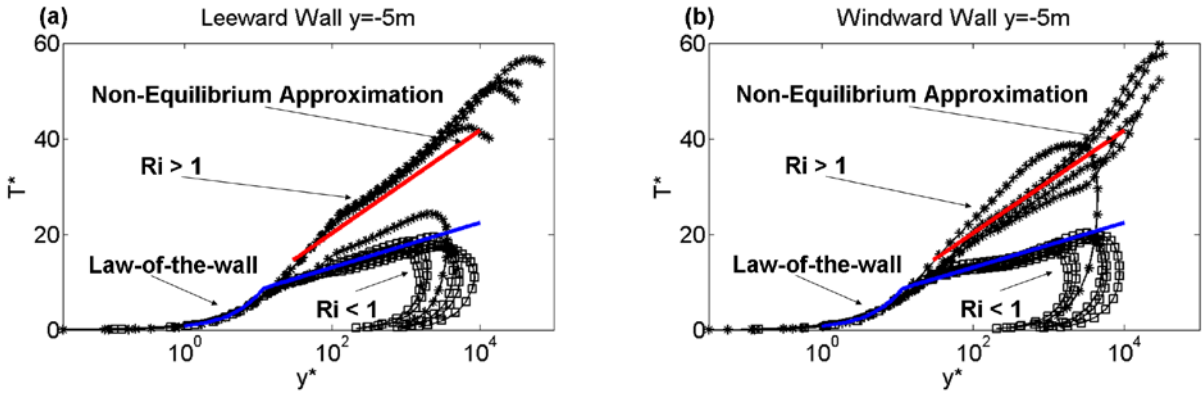

Figure 6: Dimensionless temperature profiles as a function of the y* value along the horizontal centreline (see Figure 3b) of a street canyon for simulations with different global *Ri* numbers.

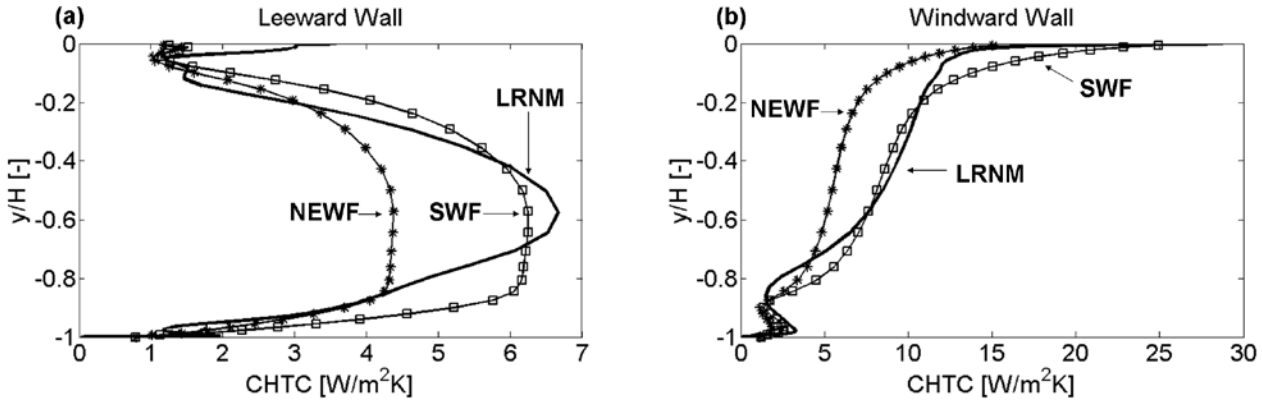

Figure 7: CHTC as a function of the vertical position y/H for a simulation with global *Ri* = 0.14. Results from SWF and NEWF are compared with LRNM.

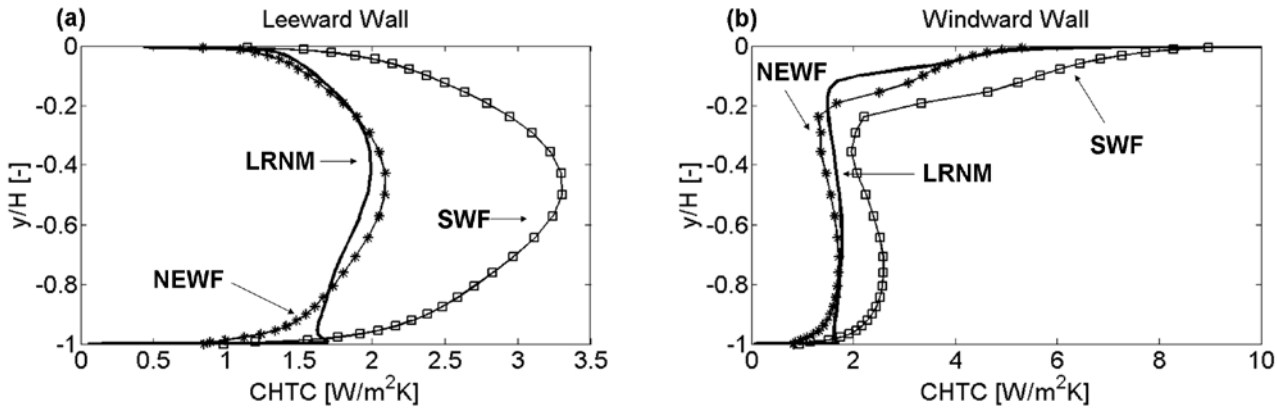

Figure 8: CHTC as a function of the vertical position y/H for a simulation with global *Ri* = 3.4. Results from SWF and NEWF are compared with LRNM.

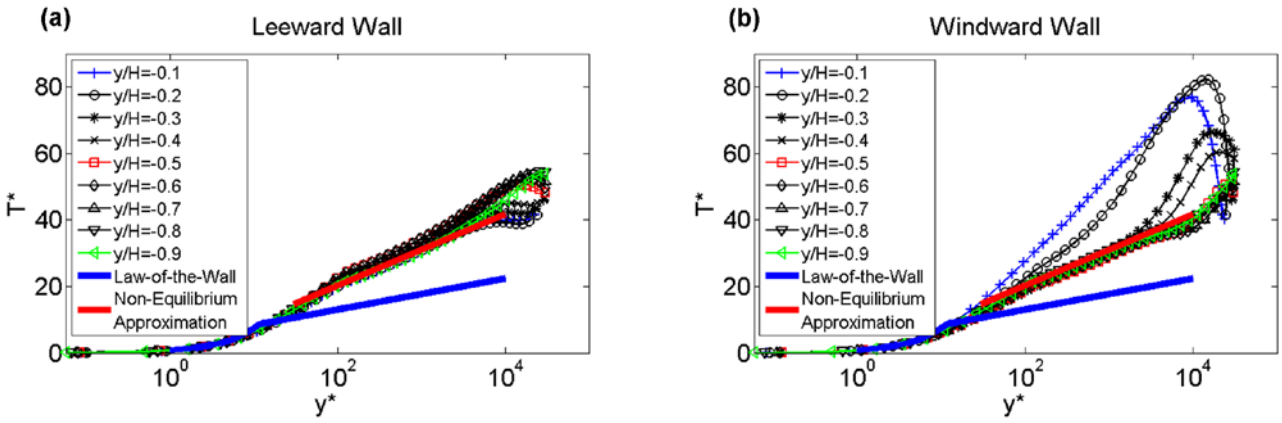

Figure 9: Dimensionless temperature profiles as a function of the *y** value on horizontal lines at different vertical positions *y/H*.

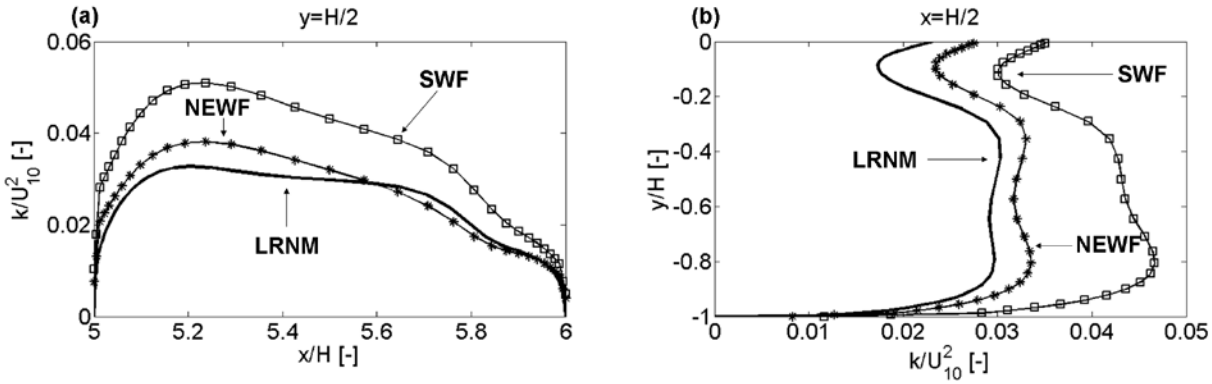

Figure 10: Turbulent kinetic energy profiles normalised by the square of the reference velocity as a function of the *x or y* position along the horizontal (a) and vertical centreline (b) (see Figure 3b). Results from simulations with SWF and NEWF are compared with result of a simulation with LRNM.

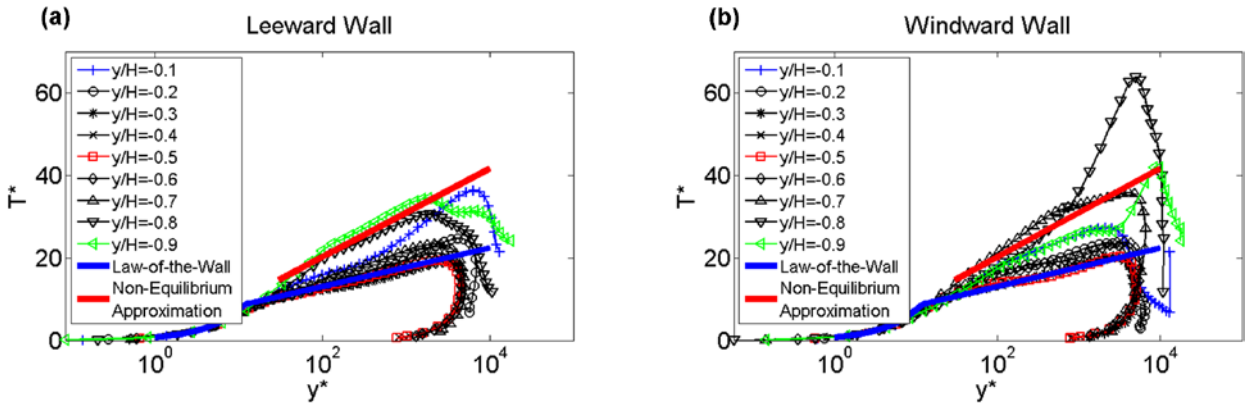

Figure 11: Dimensionless temperature profiles as a function of the *y** value on horizontal lines at different vertical positions *y/H*.

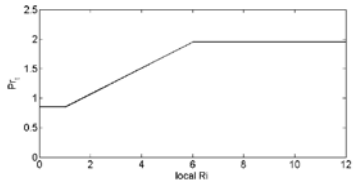

Figure 12: Turbulent wall Prandtl number as a function of the local Richardson number.

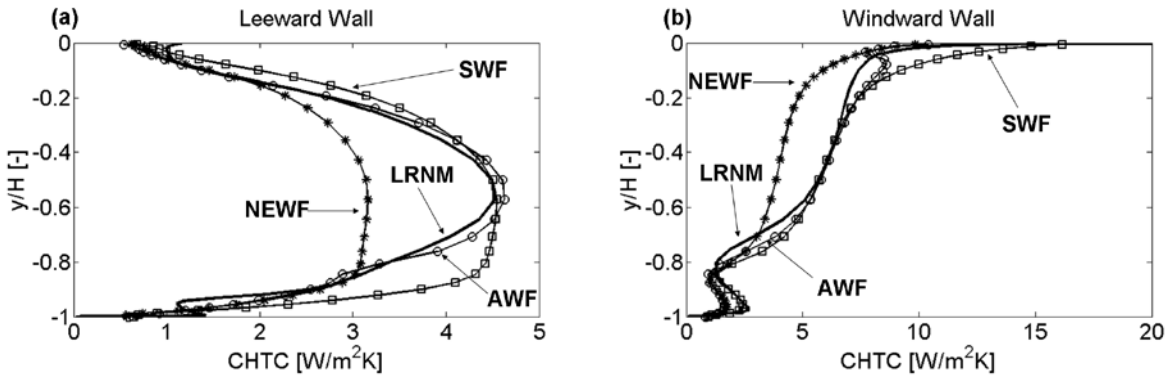

Figure 13: CHTC as a function of the vertical positions y/H for a simulation with global *Ri* = 0.38. Results from SWF, NEWF and AWF are compared with LRNM.

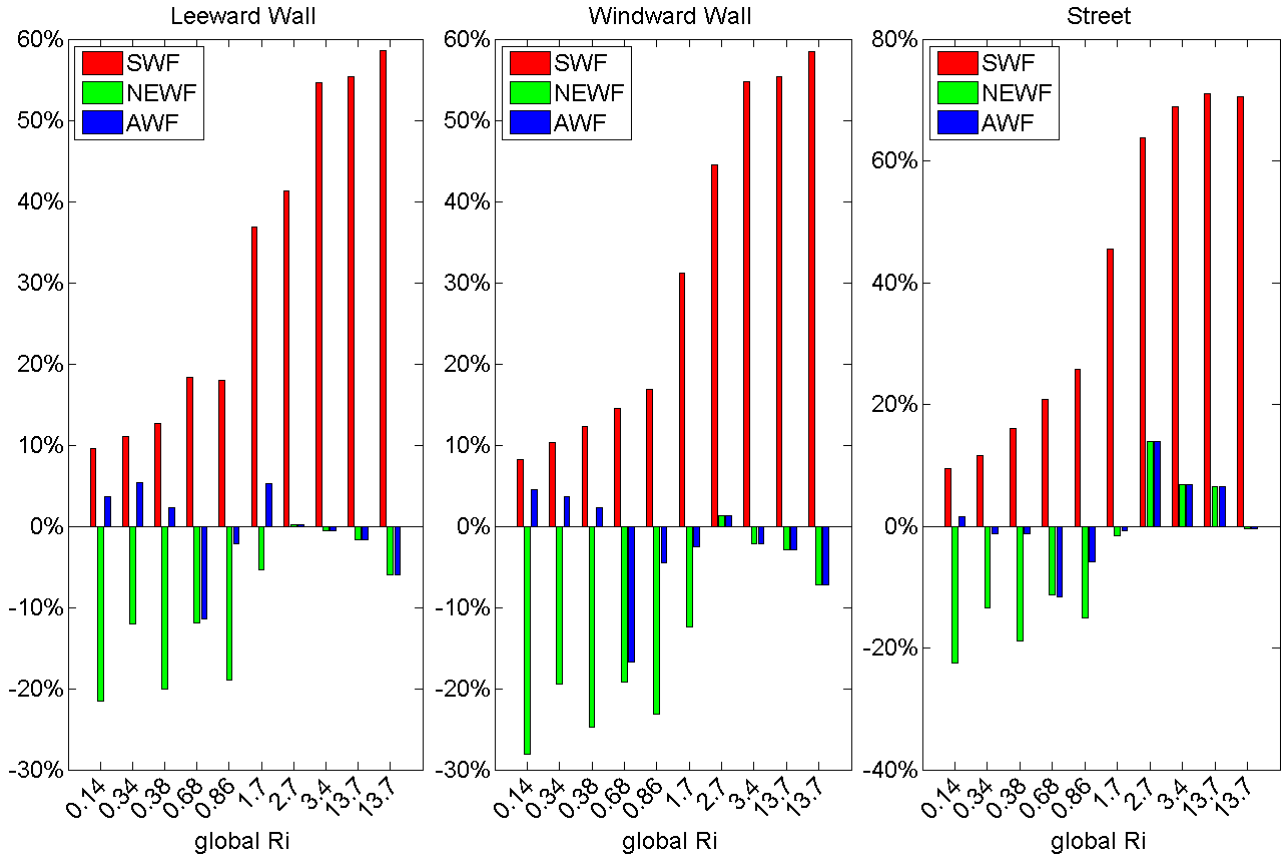

Figure 14: Relative differences of the total heat flux at the walls and the ground of the street for the SWF, NEWF and the AWF compared to the LRNM for different global *Ri*.

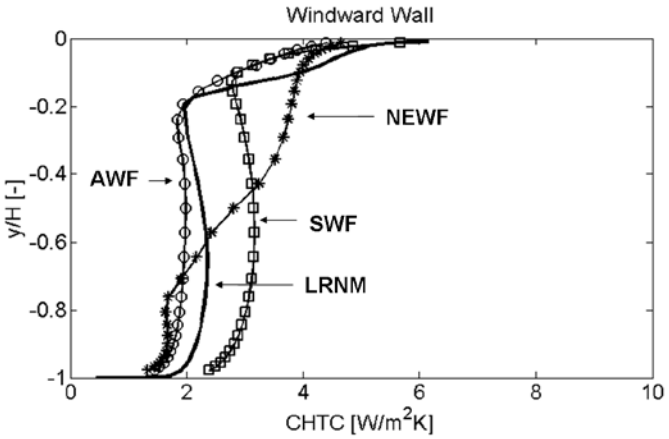

Figure 15: CHTC as a function of the vertical positions y for a simulation with a 3D street canyon with global *Ri* = 3.4. Results from simulations with SWF, NEWF and AWF are compared with result of a simulation with LRNM.

Tables

Velocity (U_{10})	5m/s	1m/s	3m/s	1m/s	2m/s	1m/s	0.5m/s	1m/s	0.5m/s	1m/s
Temperature difference	10K	1K	10K	2K	10K	5K	2K	10K	10K	40K
Ri	0.14	0.34	0.38	0.68	0.86	1.7	2.7	3.4	13.7	13.7

Table 1: Reference velocities at 10m above the ground, temperature difference between the inflow and the wall surfaces and the global Richardson number for the studied cases.